Optically Driven Collective Spin Excitations and Magnetization Dynamics in the Néel-type Skyrmion Host GaV_4S_8

P. Padmanabhan,[1,*] F. Sekiguchi,[1] R. B. Versteeg,[1] E. Slivina,[1] V. Tsurkan,[2,3] S. Bordács,[4,5] I. Kézsmárki,[3,4] and P. H. M. van Loosdrecht[1,†]

[1]*Physics Institute II, University of Cologne, 50937 Cologne, Germany*
[2]*Institute of Applied Physics, MD 2028, Chisinau, Republic of Moldova*
[3]*Experimental Physics V, Center for Electronic Correlations and Magnetism, University of Augsburg, 86159 Augsburg, Germany*
[4]*Department of Physics, Budapest University of Technology and Economics and MTA-BME Lendület Magneto-optical Spectroscopy Research Group, 1111 Budapest, Hungary*
[5]*Hungarian Academy of Sciences, Premium Postdoctoral Program, 1051 Budapest, Hungary*

(Received 27 August 2018; revised manuscript received 8 February 2019; published 15 March 2019)

GaV_4S_8 is a multiferroic semiconductor hosting magnetic cycloid (Cyc) and Néel-type skyrmion lattice (SkL) phases with a broad region of thermal and magnetic stability. Here, we use time-resolved magneto-optical Kerr spectroscopy to show the coherent generation of collective spin excitations in the Cyc and SkL phases. Our micromagnetic simulations reveal that these are driven by an optically induced modulation of uniaxial anisotropy. Our results shed light on spin dynamics in anisotropic materials hosting skyrmions and pave a new pathway for the optical manipulation of their magnetic order.

DOI: 10.1103/PhysRevLett.122.107203

The optical manipulation of topologically nontrivial phases in quantum materials [1–6] is an emerging area within condensed-matter physics [7], with efforts aimed at uncovering novel phases and exploring their nonequilibrium properties. Seminal examples include the realization of Floquet-Bloch states resulting from photon–surface-state hybridization in topological insulators [8,9] and helicity-dependent control of topological-surface currents [10]. Interest has also extended to magnetic topological defects known as skyrmions (Sks) [11], fueled by their importance in memory technology [12–14], spintronics [15], and emergent electromagnetism [16–18]. Recently, optical stimulus has been used to write and erase individual Sks [19], confirm their topological robustness [20], and identify metastable Sk states [21].

Skyrmions can be broadly classified into two varieties by their internal structure. Whirl-like Bloch-type Sks are typically found in chiral magnets [3,19,22] and are generally stable over a relatively narrow temperature range in bulk crystals. Néel-type Sks, where spins rotate in radial planes from their cores to their peripheries, have been identified in bulk lacunar spinels [23,24], tetragonal oxides [25], and thin-film heterostructures [26,27]. Notably, these systems possess a polar crystal structure exhibiting axial symmetry, in contrast to chiral magnets such as Cu_2OSeO_3. Moreover, Néel-type skyrmion lattice (SkL) states in bulk crystals of these polar magnets show an enhanced thermal stability. This stems from their orientational confinement primarily due to the pattern of the Dzyaloshinskii-Moriya interaction (DMI).

The ultrafast-optical manipulation of magnetic states can generally be accomplished by leveraging direct spin-photon coupling [28–30] or the thermal response of the host material [31,32]. At present, however, SkLs have only been coherently excited optomagnetically using the inverse-Faraday effect in the insulating Bloch-type–SkL-host Cu_2OSeO_3 [33], owing to its strong linear magneto-optical response [34]. Another possible avenue is the optical modulation of magnetic interactions (e.g., uniaxial anisotropy), which has proven successful in driving spin precessions in a variety of magnetic materials [35–39]. Within this context, lacunar spinels, possessing large uniaxial anisotropies of the easy-axis or easy-plane varieties [23,24,40,41], represent attractive targets for the optical manipulation of SkLs mediated by the energetic exchange between the electronic, lattice, and spin subsystems.

In this Letter, we report on ultrafast time-resolved magneto-optical Kerr effect (TR-MOKE) measurements that demonstrate the generation of coherent collective excitations of the magnetic Cycloid (Cyc) and SkL states in the lacunar spinel GaV_4S_8. Our results reveal GHz oscillations of the magnetization, driven by a laser-induced thermal modulation of the uniaxial anisotropy. Additionally, we observe a photoinduced enhancement of the magnetization that originates from the light-driven switching between the Cyc and SkL phases. These experiments establish an alternative route towards the optical manipulation of the dynamic magnetic character of novel spin textures, leveraging the intimate coupling between the lattice and spin degrees of freedom.

GaV_4S_8 is a multiferroic narrow-gap semiconductor belonging to a family of lacunar spinels consisting of an FCC lattice of tetrahedral $(GaS_4)^{5-}$ and cubane $(V_4S_4)^{5+}$

clusters, the latter carrying $S = 1/2$ spins. Below $T_{JT} = 44$ K, a rhombohedral (C_{3v}) Jahn-Teller distortion appears, with the rhombohedral axis oriented along one of the cubic body diagonals [42,43]. For $T < T_C \approx 13$ K [23,44] and moderate external fields, the material is an easy-axis ferromagnet with spins oriented along the rhombohedral axis. As shown in Fig. 1(a), at lower fields, a complex magnetic-phase diagram emerges consisting of Cyc and SkL phases born from the competition between the Heisenberg-exchange interaction, the DMI particular to the C_{3v} point group, and the magnetocrystalline anisotropy [23,45].

Unlike SkLs in chiral magnets, the Néel-type SkL in GaV_4S_8 is pinned to the plane perpendicular to the rhombohedral axis [23,46]. This is primarily due to the Lifshitz-invariants that comprise the DMI term, which energetically favor magnetic modulations with wave vectors perpendicular to the rhombohedral axis. Due to this and the uniaxial magnetocrystalline anisotropy, the field-stability range of the Cyc and SkL phases depend on the orientation of the magnetic field with respect to the rhombohedral axis, since different domains often coexist in these crystals. As such, several Cyc and SkL phases can be supported simultaneously, owing to the different projections of the external field along the easy axis for the four different domains. In our experiments, the external magnetic field was oriented perpendicular to an as-grown (001) surface of a GaV_4S_8 crystal identified using morphology inspection and Laue diffraction. This ensured that all the rhombohedral domains were magnetically equivalent, hosting Cyc and SkL phases over the same field ranges, as shown in Fig. 1(a) [23].

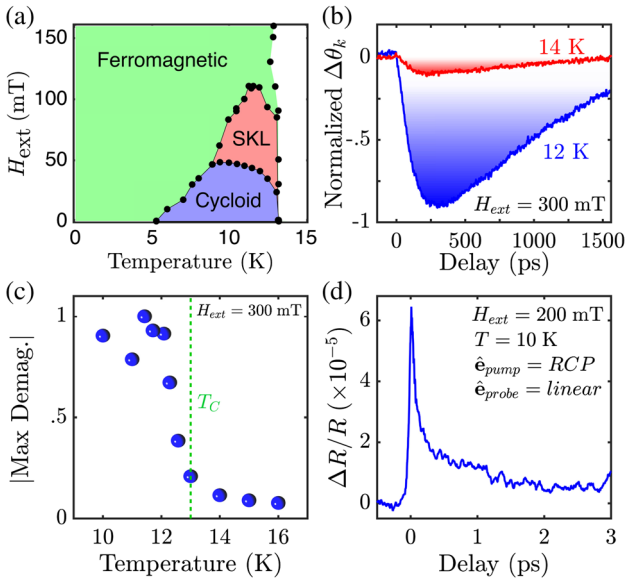

FIG. 1. (a) Magnetic phase diagram of (001) GaV_4S_8 (reproduced from Ref. [23]), (b) pump-induced change in the normalized Kerr rotation angle of the probe pulse below (blue) and above (red) T_C, (c) the absolute value of the maximum demagnetization as a function of temperature and normalized to the value at $T = 11.4$ K, and (d) the differential reflectivity trace taken at $T = 10$ K.

We employed TR-MOKE spectroscopy to probe the magnetization dynamics of the ferromagnetic, Cyc, and SkL phases. The pump and probe pulses (30 fs, 1.57 eV) were modulated at $f_{\text{pump}} = 100$ kHz and $f_{\text{probe}} = 1.87$ kHz and focused to 50 μm and 35 μm diameters, respectively. The on-sample pump fluence was 0.67 $\mu J/cm^2$. The magnetic field and sample temperature were controlled with a superconducting-magnetic cryostat. We detected the pump-induced Kerr rotation (KR) by differentially measuring the signal from the two orthogonal linear polarization components of the reflected probe beam using a phase-sensitive detection scheme locked to the intermodulation frequency between f_{pump} and f_{probe}. This method allows for rapid data acquisition, avoiding the response-time issues associated with cascaded lock-in-amplifier configurations [47].

Figure 1(b) shows the pump-induced change to the normalized KR angle ($\Delta\theta_k$) of the probe pulse for the ferromagnetic (blue trace) and paramagnetic (red trace) phases. As seen in Fig. 1(c), the magnitude of the demagnetization step dramatically increases below T_C, consistent with the onset of ferromagnetic order. We found that the demagnetization occurred over ~200 ps for all external fields and sample temperatures that coincide with the ferromagnetic phase. This timescale is consistent with other semiconducting ferromagnets and is attributed to the slow thermalization of the spin system due to its coupling to the lattice and isolation from the electronic bath [48,49]. This is supported by the differential-reflectivity trace shown in Fig. 1(d), which contains contributions from electron-electron, electron-phonon, and phonon-phonon scattering [50,51], all of which reach quasiequilibrium within a few picoseconds. The change in $\Delta\theta_k$ occurs on a much longer timescale, demonstrated by its relatively small variation during the first few picoseconds. Accordingly, the thermalization of the phonon bath is a nearly instantaneous event for the spins and the timescale of the demagnetization is primarily governed by the strength of the magnon-phonon coupling [52,53].

The slow response of the spin-system to changes in the lattice is further exemplified by the magnetization dynamics just below T_C. Figure 2 shows the time derivative of $\Delta\theta_k$ at $T = 12$ K for different external magnetic fields (H_{ext}). For $H_{\text{ext}} \geq 35$ mT (SkL phase), we observe demagnetization dynamics. However, for $H_{\text{ext}} \leq 30$ mT (Cyc phase), the signal increases following the pump pulse. This photo-induced enhancement of the magnetization originates from the temperature dependence of the magnetization (M) across the magnetic phase boundaries [54]. The inset of Fig. 2 shows $M(T)$ normal to the (001) surface for $H_{\text{ext}} = 30$ mT and 50 mT measured using a SQUID magnetometer. As indicated by the arrow, the 30-mT curve is peaked at the Cyc and SkL phase boundary above 12 K.

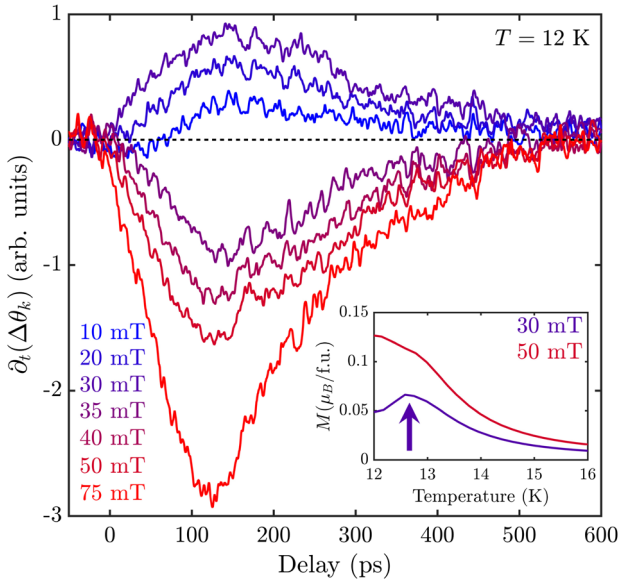

FIG. 2. Time derivative of the TR-MOKE signal at $T = 12$ K at various external magnetic fields. The inset shows the temperature dependence of the magnetization for $H_{ext} = 30$ mT (purple) and 50 mT (red). The arrow marks the peak at the Cyc and SkL interface.

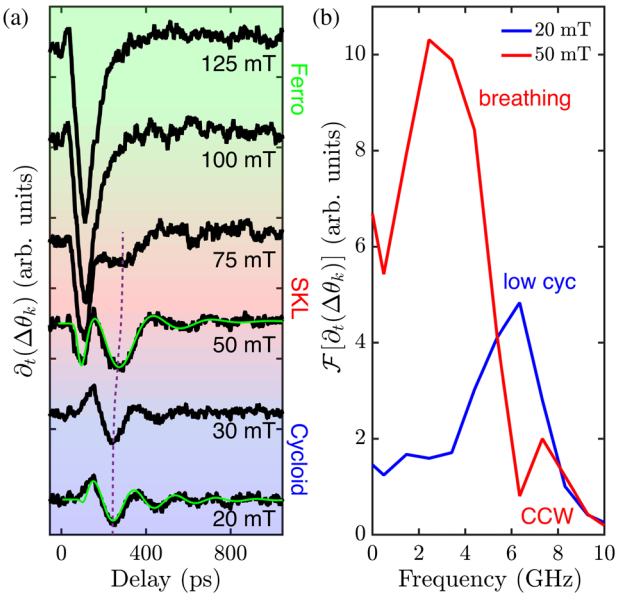

FIG. 3. (a) Time derivative of the TR-MOKE signal at $T = 10$ K for different external magnetic fields spanning the Cyc, SkL, and ferromagnetic phases and (b) the Fourier transforms of the 20 mT (blue) and 50 mT (red) traces in (a). The dashed line in (a) marks the end of the first oscillatory period. The green lines in (a) are calculated using Eqs. (2) and (3) with $\beta = 0.02$ and $\gamma = 0.135$ ($\beta = 0.1$ and $\gamma = 0.25$) for the 20 mT (50 mT) curve.

Accordingly, the enhancement of the magnetization results from the comparatively slow response of the spins to the impulsive heating of the lattice, pushing the system along the $M(T)$ peak following the pump excitation. At higher fields, the peak in $M(T)$ vanishes, as shown in the 50-mT curve, reflecting the restoration of demagnetization behavior.

To probe the dynamics of the Cyc and SkL phases, we set $T = 10$ K and collected TR-MOKE traces for several external magnetic fields. The results are shown as black lines in Fig. 3(a), where we plot the derivative of $\Delta\theta_k$ to suppress the incoherent magnetization dynamics. For small fields, we observe GHz oscillations, as seen in the 20–75 mT traces. With increasing field, the oscillation frequency changes, as noted by the dashed line marking the end of the first oscillatory period. For $H_{ext} > 75$ mT, the oscillatory structure vanishes. Figure 3(b) shows Fourier transforms of two traces in Fig. 3(a), representative of the Cyc phase (20 mT) and the SkL phase (50 mT). In the Cyc phase, we see a single peak centered at approximately 6 GHz. Comparing this to ESR measurements [40], we identify this as the low-frequency Cyc eigenmode. In the SkL phase, we observe a strong peak centered at 3.75 GHz and a weaker peak at 7.50 GHz. These frequencies are consistent with the SkL breathing mode and the counterclockwise (CCW) rotation mode, respectively [40]. Notably, the clockwise (CW) rotation mode is absent in our measurements.

We now address two fundamental questions: (1) what is the mechanism driving the coherent collective spin excitations and (2) why are only certain modes excited? To answer the first, we note that the presence of coherent Cyc or SkL excitations was invariant to the choice of pump polarization. This is typically a fingerprint of a thermal process that does not involve a direct coupling between the pump-photons and the spin system [31]. Thermal mechanisms of this type have been explored in the study of laser-induced spin-precessions in materials such as $TmFeO_3$ [35], Co films [36], and GaMnAs [37,38].

Being a polar semiconductor, the electron and optical phonon subsystems in GaV_4S_8 are strongly coupled, leading to a substantial increase in the lattice temperature following the pump pulse [50]. This can, in turn, cause a modulation of the magnetocrystalline anisotropy [31]. Though such an effect typically requires a large pump fluence, this constraint is eased in GaV_4S_8 due to the strong temperature variation of its first uniaxial anisotropy constant (K_1) below T_C [41]. Therefore, the laser-induced heating of the sample significantly modulates the effective field acting on the magnetic system through the anisotropy contribution, driving the magnetic excitations of the SkL and Cyc states. Owing to the relatively long time required for heat to dissipate from the photoexcited volume through diffusion [50], this manifests as a step-like modulation of K_1 within the experimental window.

To justify the above description, we used the finite-difference time-domain method to solve the Landau-Lifshitz-Gilbert equation for the SkL state using MUMAX3 [55]. The effective field acting on the magnetic system is given by

$$\begin{aligned}\mathbf{H}_{\text{eff}} &= \mathbf{H}_{\text{ext}} + \mathbf{H}_{\text{ani}} + \mathbf{H}_d + \mathbf{H}_{\text{DMI}} + \mathbf{H}_{\text{exch}} \\ &= H_{\text{ext}}\hat{\mathbf{e}}_{\text{ext}} + \frac{2K_1}{\mu_0 M_S}(\hat{\mathbf{e}}_u \cdot \mathbf{m})\hat{\mathbf{e}}_u + \mathbf{H}_d \\ &\quad + \frac{2D}{\mu_0 M_S}[\mathcal{L}_{xz}^{(x)} + \mathcal{L}_{yz}^{(y)}] + \frac{2A_{\text{ex}}}{\mu_0 M_S}\nabla^2\mathbf{m} \qquad (1)\end{aligned}$$

where $A_{\text{ex}} = 0.0588$ pJ/m is the exchange stiffness, $M_S = 28.8$ kA/m is the saturation magnetization, $K_1 = 10$ kJ/m^3 is the (steady-state) anisotropy constant, $D = 0.043$ mJ/m^2 is the DMI constant, $\mathcal{L}_{jk}^{(i)} = m_j\partial_i m_k - m_k\partial_i m_j$ are Lifshitz invariants corresponding to C_{3v} symmetry, $\hat{\mathbf{e}}_u$ is a unit vector in the direction of the easy axis, $\hat{\mathbf{e}}_{\text{ext}}$ is a unit vector in the direction of the applied field, $\mathbf{m} = \mathbf{M}/M_S$, and $\mathbf{H}_d$ is the demagnetizing field. The material parameters were estimated from literature and match the experimental periodicity of the SkL state [23,41]. Here, $\hat{\mathbf{x}}'\|[100]$, $\hat{\mathbf{y}}'\|[010]$, $\hat{\mathbf{z}}'\|[001]$, $\hat{\mathbf{x}}\|[11\bar{2}]$, $\hat{\mathbf{y}}\|[1\bar{1}0]$, and $\hat{\mathbf{z}} = \hat{\mathbf{e}}_u\|[111]$. We introduced a time dependence in the effective field through a steplike decrease of K_1 by 1% of its steady-state value, consistent with our estimate of the pump-induced heating of the lattice.

Before simulating the SkL magnetization dynamics, we verified the stability of the SkL phase for the parameters listed above by cooling a 512×512 cuboid grid with a randomized initial magnetization simultaneously subjected to both static and thermally fluctuating magnetic fields [55,56]. We then used a 128×64 grid with periodic boundary conditions along $\hat{\mathbf{x}}$ and $\hat{\mathbf{y}}$, initialized with one unit cell of a triangular Néel-type SkL (SkL plane $\perp \hat{\mathbf{z}}$) for the SkL dynamics simulations. The lattice parameters associated with the SkL were obtained by minimizing the total energy density of the equilibrium configuration. Details of this process are provided in the Supplemental Material [57]. For the results discussed below, the external field parallel to $\hat{\mathbf{z}}$ was 125 mT and the field along $\hat{\mathbf{x}}$ was varied, resulting in an increase in magnitude and tilting of the external field with respect to $\hat{\mathbf{e}}_u$ by an angle α.

Figure 4(a) shows the Fourier transforms of $\dot{m}_z$, $\dot{m}_x$, and $\dot{m}_{z'}$ for various values of α. For $\alpha = 0°$, a single resonance peak appears only in the z component, corresponding to the breathing mode. This is because the modulation of $\mathbf{H}_{\text{eff}}$ is entirely along $\hat{\mathbf{z}}$ (i.e., normal to the SkL plane) and can therefore only couple to the breathing mode [58]. As α is increased, however, we see two additional peaks emerge in the z, x, and z' components of the magnetization. The appearance of the new resonances is due to the core-shift characteristic of Néel-type SkLs subject to oblique external fields [59]. This results in a deformation of the Sk texture, reducing the sixfold rotational symmetry of the SkL to a twofold rotation, thereby introducing a time-dependent component to the effective field in the SkL plane, exciting the rotational modes [58]. The tilting of the net magnetization and deformation of the SkL are relatively small, which accounts for the weakness of the CCW mode in our measurements where $\alpha = 54.7°$. Further, we see that the third simulated resonance is relatively weak, a fact that is supported by the absence of the CW mode in our measurements. Finally, we note that the simulated resonances were blueshifted with respect to the experimental results. This deviation is most likely due to the strong sensitivity of the mode frequencies to the values of D and A_{ex} [56]. This is also the most likely cause of the higher external fields required to stabilize the SkL phase in the simulations relative to the experiments. Nevertheless, the order of the simulated resonances is consistent with previous ESR measurements [40] as well as our experimental observations.

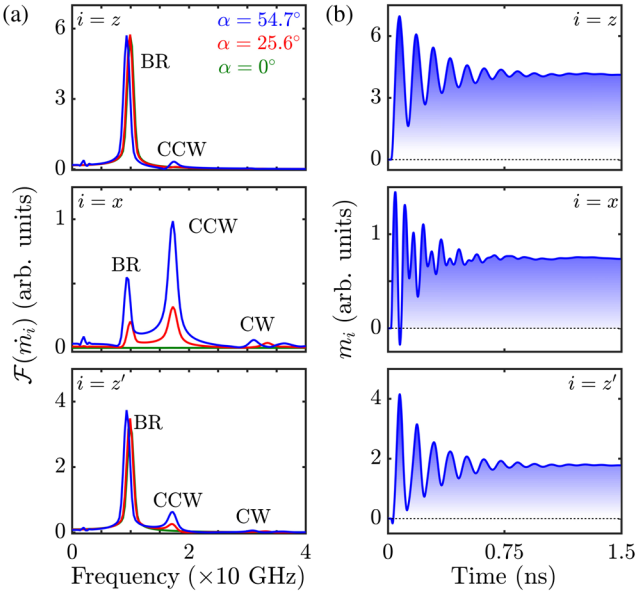

FIG. 4. (a) The Fourier transforms of the simulated $\dot{m}_z$, $\dot{m}_x$, and $\dot{m}_{z'}$ for various values of α spanned by the external magnetic field and the rhombohedral axis and (b) the simulated $m_z(t)$, $m_x(t)$, and $m_{z'}(t)$ for $\alpha = 54.7°$.

We now construct a phenomenological model of the experimental TR-MOKE signals. From Fig. 4(b), we see that the magnetization dynamics resulting from a modulation of K_1 are comprised of decaying sinusoidal oscillations superimposed on a steplike offset. This reflects the transient reorientation of the magnetization due to the reduced anisotropy following the optical pump. This type of response can be modeled by a damped harmonic oscillator driven by a steplike force, here representing the optically induced modulation of the uniaxial anisotropy. The incoherent demagnetization and remagnetization dynamics can be described by the sum of two exponentials convolved with a steplike function representing the response of the spin system to the lattice. For both the oscillatory and incoherent parts, we use the same steplike function. Finally, we model the magnetization dynamics as the sum of the incoherent (I_i) and oscillatory (I_o) contributions, taking $\Delta\theta(t) = A \cdot I_i(t) + B \cdot I_o(t)$. I_o and I_i are given by the solutions to

$$\frac{d^2 I_o}{dt^2} + 2\gamma\omega_0 \frac{dI_o}{dt} + \omega_o^2 I_o = g(t)e^{-t/\tau}, \quad (2)$$

$$I_i(t) = (h * g)(t) \quad (3)$$

where $h(t) = e^{-t/\tau_1} - \beta e^{-t/\tau_2}$, $g(t) = [\mathrm{erf}(\alpha t) + 1]$, and γ is the oscillator damping ratio. Here, τ_1 and τ_2 are the demagnetization and remagnetization time constants, β is a scaling parameter, α controls the spin-response time, and τ is the rate at which K_1 returns to the pre-time-zero value. Estimating $\tau_1 = 130$ ps, $\tau_2 = \tau = 2600$ ps, and $\alpha = 0.05$ from the experimental results, we obtain the curves plotted in green in Fig. 3(a). The agreement between this model and our measurements illustrates that the measured magnetization dynamics reflect the competition between incoherent and oscillatory signals.

In summary, we have demonstrated the ultrafast optical generation of coherent collective spin excitations of the Cyc and SkL phases in GaV_4S_8, driven by an optically induced modulation of the uniaxial magnetocrystalline anisotropy. This indirect coupling between the optical pulse and the spin system is mediated by the lattice and represents a new mechanism by which magnetic excitations can be generated in skyrmion-host compounds with strong anisotropy. Furthermore, the peculiar nature of the magnetic ordering at the phase boundaries of GaV_4S_8 allows for a transient enhancement of the magnetization driven by the optically induced heating of the lattice. This Letter underscores the intimate coupling between the spin and lattice subsystems in GaV_4S_8, and may provide a stepping stone towards the optical control of topological magnetic objects in semiconductors.

P. P., F. S., R. B. V., E. S., and P. H. M. vL. acknowledge financial support from the Deutsche Forschungsgemeinschaft (DFG) through SFB-1238 (Project B05). V. T. and I. K. acknowledge financial support from the DFG via the Transregional Research Collaboration TRR 80: From Electronic Correlations to Functionality (Augsburg-Munich-Stuttgart) and via the Skyrmionics Priority Program SPP2137. S. B. acknowledges financial support from the National Research, Development and Innovation Office—NKFIH, ANN 122879, and the BME-Nanotechnology and Materials Science FIKP grant of EMMI (BME FIKP-NAT).

*prashpad@lanl.gov
Current address: Center for Integrated Nanotechnologies, Los Alamos National Laboratory, Los Alamos, New Mexico 87545, USA
†pvl@ph2.uni-koeln.de

[1] D. Hsieh, D. Qian, L. Wray, Y. Xia, Y. S. Hor, R. J. Cava, and M. Z. Hasan, Nature (London) **452**, 970 (2008).
[2] X. Z. Yu, N. Kanazawa, Y. Onose, K. Kimoto, W. Z. Zhang, S. Ishiwata, Y. Matsui, and Y. Tokura, Nat. Mater. **10**, 106 (2011).
[3] T. Adams, A. Chacon, M. Wagner, A. Bauer, G. Brandl, B. Pedersen, H. Berger, P. Lemmens, and C. Pfleiderer, Phys. Rev. Lett. **108**, 237204 (2012).
[4] Z. K. Liu, B. Zhou, Y. Zhang, Z. J. Wang, H. M. Weng, D. Prabhakaran, S.-K. Mo, Z. X. Shen, Z. Fang, X. Dai, Z. Hussain, and Y. L. Chen, Science **343**, 864 (2014).
[5] B. Q. Lv, H. M. Weng, B. B. Fu, X. P. Wang, H. Miao, J. Ma, P. Richard, X. C. Huang, L. X. Zhao, G. F. Chen, Z. Fang, X. Dai, T. Qian, and H. Ding, Phys. Rev. X **5**, 031013 (2015).
[6] S.-Y. Xu *et al.*, Science **349**, 613 (2015).
[7] D. N. Basov, R. D. Averitt, and D. Hsieh, Nat. Mater. **16**, 1077 (2017).
[8] Y. H. Wang, H. Steinberg, P. Jarillo-Herrero, and N. Gedik, Science **342**, 453 (2013).
[9] M. C. Rechtsman, J. M. Zeuner, Y. Plotnik, Y. Lumer, D. Podolsky, F. Dreisow, S. Nolte, M. Segev, and A. Szameit, Nature (London) **496**, 196 (2013).
[10] C. Kastl, C. Karnetzky, H. Karl, and A. W. Holleitner, Nat. Commun. **6**, 6617 (2015).
[11] N. Nagaosa and Y. Tokura, Nat. Nanotechnol. **8**, 899 (2013).
[12] A. Fert, V. Cros, and J. Sampaio, Nat. Nanotechnol. **8**, 152 (2013).
[13] R. Tomasello, E. Martinez, R. Zivieri, L. Torres, M. Carpentieri, and G. Finocchio, Sci. Rep. **4**, 6784 (2015).
[14] G. Yu, P. Upadhyaya, Q. Shao, H. Wu, G. Yin, X. Li, C. He, W. Jiang, X. Han, P. K. Amiri, and K. L. Wang, Nano Lett. **17**, 261 (2017).
[15] A. Rosch, Nat. Nanotechnol. **12**, 103 (2016).
[16] T. Schulz, R. Ritz, A. Bauer, M. Halder, M. Wagner, C. Franz, C. Pfleiderer, K. Everschor, M. Garst, and A. Rosch, Nat. Phys. **8**, 301 (2012).
[17] A. Neubauer, C. Pfleiderer, B. Binz, A. Rosch, R. Ritz, P. G. Niklowitz, and P. Böni, Phys. Rev. Lett. **102**, 186602 (2009).
[18] R. Ritz, M. Halder, C. Franz, A. Bauer, M. Wagner, R. Bamler, A. Rosch, and C. Pfleiderer, Phys. Rev. B **87**, 134424 (2013).
[19] G. Berruto, I. Madan, Y. Murooka, G. M. Vanacore, E. Pomarico, J. Rajeswari, R. Lamb, P. Huang, A. J. Kruchkov, Y. Togawa, T. LaGrange, D. McGrouther, H. M. Rønnow, and F. Carbone, Phys. Rev. Lett. **120**, 117201 (2018).
[20] M. C. Langner, S. Roy, S. W. Huang, J. D. Koralek, Y.-D. Chuang, G. L. Dakovski, J. J. Turner, J. S. Robinson, R. N. Coffee, M. P. Minitti, S. Seki, Y. Tokura, and R. W. Schoenlein, Phys. Rev. Lett. **119**, 107204 (2017).
[21] T. Eggebrecht, M. Möller, J. G. Gatzmann, N. Rubiano da Silva, A. Feist, U. Martens, H. Ulrichs, M. Münzenberg, C. Ropers, and S. Schäfer, Phys. Rev. Lett. **118**, 097203 (2017).
[22] A. Tonomura, X. Yu, K. Yanagisawa, T. Matsuda, Y. Onose, N. Kanazawa, H. S. Park, and Y. Tokura, Nano Lett. **12**, 1673 (2012).
[23] I. Kézsmárki, S. Bordács, P. Milde, E. Neuber, L. M. Eng, J. S. White, H. M. Rønnow, C. D. Dewhurst, M. Mochizuki, K. Yanai, H. Nakamura, D. Ehlers, V. Tsurkan, and A. Loidl, Nat. Mater. **14**, 1116 (2015).
[24] S. Bordács, A. Butykai, B. G. Szigeti, J. S. White, R. Cubitt, A. O. Leonov, S. Widmann, D. Ehlers, H.-A. K. von Nidda, V. Tsurkan, A. Loidl, and I. Kézsmárki, Sci. Rep. **7**, 7584 (2017).

[25] T. Kurumaji, T. Nakajima, V. Ukleev, A. Feoktystov, T.-h. Arima, K. Kakurai, and Y. Tokura, Phys. Rev. Lett. **119**, 237201 (2017).
[26] G. Chen, A. Mascaraque, A. T. N'Diaye, and A. K. Schmid, Appl. Phys. Lett. **106**, 242404 (2015).
[27] S. D. Pollard, J. A. Garlow, J. Yu, Z. Wang, Y. Zhu, and H. Yang, Nat. Commun. **8**, 14761 (2017).
[28] J. Zhao, A. V. Bragas, D. J. Lockwood, and R. Merlin, Phys. Rev. Lett. **93**, 107203 (2004).
[29] R. Iida, T. Satoh, T. Shimura, K. Kuroda, B. A. Ivanov, Y. Tokunaga, and Y. Tokura, Phys. Rev. B **84**, 064402 (2011).
[30] C. Tzschaschel, K. Otani, R. Iida, T. Shimura, H. Ueda, S. Günther, M. Fiebig, and T. Satoh, Phys. Rev. B **95**, 174407 (2017).
[31] A. Kirilyuk, A. V. Kimel, and T. Rasing, Rev. Mod. Phys. **82**, 2731 (2010).
[32] H. Shibata, M. Okano, and S. Watanabe, Phys. Rev. B **97**, 014438 (2018).
[33] N. Ogawa, S. Seki, and Y. Tokura, Sci. Rep. **5**, 9552 (2015).
[34] R. B. Versteeg, I. Vergara, S. D. Schäfer, D. Bischoff, A. Aqeel, T. T. M. Palstra, M. Grüninger, and P. H. M. van Loosdrecht, Phys. Rev. B **94**, 094409 (2016).
[35] A. V. Kimel, A. Kirilyuk, A. Tsvetkov, R. V. Pisarev, and T. Rasing, Nature (London) **429**, 850 (2004).
[36] J.-Y. Bigot, M. Vomir, L. Andrade, and E. Beaurepaire, Chem. Phys. **318**, 137 (2005).
[37] J. Wang, I. Cotoros, K. M. Dani, X. Liu, J. K. Furdyna, and D. S. Chemla, Phys. Rev. Lett. **98**, 217401 (2007).
[38] Y. Hashimoto, S. Kobayashi, and H. Munekata, Phys. Rev. Lett. **100**, 067202 (2008).
[39] H. Shibata, M. Okano, and S. Watanabe, Phys. Rev. B **97**, 014438 (2018).
[40] D. Ehlers, I. Stasinopoulos, V. Tsurkan, H.-A. Krug von Nidda, T. Fehér, A. Leonov, I. Kézsmárki, D. Grundler, and A. Loidl, Phys. Rev. B **94**, 014406 (2016).
[41] D. Ehlers, I. Stasinopoulos, I. Kézsmárki, T. Fehér, V. Tsurkan, H.-A. K. von Nidda, D. Grundler, and A. Loidl, J. Phys. Condens. Matter **29**, 065803 (2017).
[42] Z. Wang, E. Ruff, M. Schmidt, V. Tsurkan, I. Kézsmárki, P. Lunkenheimer, and A. Loidl, Phys. Rev. Lett. **115**, 207601 (2015).
[43] J. Hlinka, F. Borodavka, I. Rafalovskyi, Z. Docekalova, J. Pokorny, I. Gregora, V. Tsurkan, H. Nakamura, F. Mayr, C. A. Kuntscher, A. Loidl, S. Bordács, D. Szaller, H.-J. Lee, J. H. Lee, and I. Kézsmárki, Phys. Rev. B **94**, 060104 (2016).
[44] H. Nakamura, H. Chudo, and M. Shiga, J. Phys. Condens. Matter **17**, 6015 (2005).
[45] A. Bogdanov and A. Hubert, J. Magn. Magn. Mater. **138**, 255 (1994).
[46] J. S. White, Á. Butykai, R. Cubitt, D. Honecker, C. D. Dewhurst, L. F. Kiss, V. Tsurkan, and S. Bordács, Phys. Rev. B **97**, 020401 (2018).
[47] J. Wang, in *Optical Techniques for Solid-state Materials Characterization*, edited by R. P. Prasankumar and A. J. Taylor (CRC Press, Boca Raton, 2012), Chap. 13, pp. 467–506.
[48] E. Kojima, R. Shimano, Y. Hashimoto, S. Katsumoto, Y. Iye, and M. Kuwata-Gonokami, Phys. Rev. B **68**, 193203 (2003).
[49] J. Wang, C. Sun, Y. Hashimoto, J. Kono, G. A. Khodaparast, Ł. Cywiński, L. J. Sham, G. D. Sanders, C. J. Stanton, and H. Munekata, J. Phys. Condens. Matter **18**, R501 (2006).
[50] A. Othonos, J. Appl. Phys. **83**, 1789 (1998).
[51] P. Y. Yu and M. Cardona, *Fundamentals of Semiconductors*, 4th ed. (Springer-Verlag, New York, 2010), pp. 292–295.
[52] C. Kittel, Phys. Rev. **110**, 836 (1958).
[53] A. V. Kimel, R. V. Pisarev, J. Hohlfeld, and T. Rasing, Phys. Rev. Lett. **89**, 287401 (2002).
[54] E. Ruff, S. Widmann, P. Lunkenheimer, V. Tsurkan, S. Bordacs, I. Kezsmarki, and A. Loidl, Sci. Adv. **1**, e1500916 (2015).
[55] A. Vansteenkiste, J. Leliaert, M. Dvornik, M. Helsen, F. Garcia-Sanchez, and B. Van Waeyenberge, AIP Adv. **4**, 107133 (2014).
[56] V. L. Zhang, C. G. Hou, K. Di, H. S. Lim, S. C. Ng, S. D. Pollard, H. Yang, and M. H. Kuok, AIP Adv. **7**, 055212 (2017).
[57] See Supplemental Material at http://link.aps.org/supplemental/10.1103/PhysRevLett.122.107203 for information regarding the finite-difference time-domain simulations, verification of the SkL-phase stability, the procedure used to obtain the lattice parameters utilized in the simulations, and simulated plots of the SkL deformation under oblique external magnetic fields.
[58] M. Mochizuki, Phys. Rev. Lett. **108**, 017601 (2012).
[59] A. O. Leonov and I. Kézsmárki, Phys. Rev. B **96**, 214413 (2017).